Sol-gel-derived titanium oxide–cerium oxide biocompatible nanocomposite film for urea sensor

Anees A. Ansari, G. Sumana, M.K. Pandey, and B.D. Malhotra[a)]
Biomolecular Electronics & Conducting Polymer Research Group, National Physical Laboratory, New Delhi-110012, India

(Received 6 May 2008; accepted 3 October 2008)

Sol-gel-derived biocompatible titanium oxide–cerium oxide (TiO_2–CeO_2) nanocomposite film was deposited onto indium tin oxide (ITO)-coated glass substrate by the dip-coating method. This nanobiocomposite film has been characterized using x-ray diffraction, Fourier transform infrared, atomic force microscope, and electrochemical techniques, respectively. The particle size of the TiO_2–CeO_2 nanobiocomposite film was found to be 23 nm. The urea biosensor fabricated by immobilizing mixed enzyme [urease (Urs) and glutamate dehydrogenase (GLDH)] on this nanobiocomposite showed a response time of 10 s, sensitivity as 0.9165 $\mu Acm^{-2}mM^{-1}$, detection limit of 0.166 μM, and negligible effect due to interferants uric acid, cholesterol, glucose, and ascorbic acid. The value of Michaelis–Menten constant (K_m) estimated using Lineweaver–Burke plot as 4.8 mM indicated enhancement in the affinity and/or activity of enzyme attached to their nanobiocomposite. This bioelectrode retained 95% of enzyme activity after 6 months at 4 °C.

I. INTRODUCTION

The recent past has seen numerous investigations carried out on development and improvements on various features, such as speed, selectivity and sensitivity, and reduced cost of electrochemical biosensors.[1,2] Many metal oxide-based nanomaterials, such as zinc oxide (ZnO),[3–5] zirconium oxide (ZrO_2),[6,7] tin oxide (SnO_2),[8] titanium oxide (TiO_2),[9,10] niobium oxide (Nb_2O_5),[11] and cerium oxide (CeO_2),[12] etc., have been used as immobilization matrices for the development of biosensors. Among those, nanostructured TiO_2 has received much attention as an immobilization matrix for the design of desired biosensors because of its one-dimensional nanostructure, electronic conductivity, and larger specific surface area.[13] It has been reported that the presence of higher valence cationic (4^+) dopants enhances the ionic conductivity of TiO_2 due to increase in the concentration of oxygen vacancies.[14,15] It was suggested that partial orientation of TiO_2 nanoparticles may have an influence on ionic conductivity of this material near the surface.[16] These features are particularly attractive as potential adsorbents for enzyme immobilization as ambient temperature necessitates further development of new catalytic materials with a high surface area and well-defined reactive crystal planes with superior catalytic activity.

Efforts have recently been made to tailor the catalytic properties of TiO_2 by the addition of CeO_2 to enhance thermal and electrical properties, and these novel materials have been exploited for applications toward passive counter electrodes and sensors.[14,15,17] In recent years, a number of sol-gel-derived oxide substrates were used for improving characteristics of biosensors for detection of various analytes.[3,4,13,17–22] Various techniques, such as radio frequency (rf) sputtering, electrochemical deposition, and sol-gel techniques, have been used to prepare TiO_2–CeO_2 composite thin films.[14–24] Among sol-gel-derived oxide substrates, TiO_2–CeO_2 films have acquired much attention in biomedical applications due to various advantages, such as low temperature process ability, large surface area, tunability, thermal stability, biocompatibility, and low cost.[13,18,20,23] Titanium oxide sol-gel films have been used to immobilize horseradish peroxidase (HRP) for application to H_2O_2 biosensor.[8,13,26,27] In addition, sol-gel-derived tin oxide/gelatin composite films were used to investigate direct electrochemistry and electrocatalysis of horseradish peroxidase.[23] Furthermore, this sol-gel-derived zirconia/nafion composite has been used to fabricate glucose biosensor.[28]

Urea in blood or in urine is an important analyte for the diagnosis of renal and liver diseases. The detection of urea is performed frequently in medical care. The normal level of urea in serum is in the range 2.5–6.7 mM (15–45 mg/dL). In patients suffering from renal disease, urea concentration in serum may be as high as 30–80 mM necessitating hemodialysis.[29]

[a)]Address all correspondence to this author.
e-mail: bansi.malhotra@gmail.com
DOI: 10.1557/JMR.2009.0212

We report preparation, characterization, and application of sol-gel-derived TiO_2–CeO_2 film for fabrication of urea biosensor.

II. EXPERIMENTAL

A. Chemicals and reagents

Urease (Urs), glutamate dehydrogenase (GLDH), nicotinamide adenine dinucleotide (NADH) α-keto glutarate (α-KG), titanium butoxide, Na_2HPO_4, and NaH_2PO_4 were procured from Sigma Aldrich (St. Louis, MO). $(NH_4)_2Ce(NO_3)_6$, ethanol, NH_4OH, HNO_3, solvents, and reagents were procured from Merck India Ltd., Mumbai, India. All of these chemicals were of analytical grade and used without further purification. Indium tin oxide (ITO)-coated glass substrates were obtained from Balzers, UK. The deionized water obtained from Millipore water purification system (Milli Q 10 TS, US) was used for the preparation of solutions and buffers.

B. Deposition of sol-gel nanostructured TiO_2–CeO_2 films

Mixed TiO_2–CeO_2 thin films were deposited on precleaned ITO-coated glass substrates by sol-gel process using the dip-coating technique.[18] The sol was prepared by mixing cerium ammonium nitrate (100 mg) solution in ethanol (20 mL) with titanium butoxide (900 mg) in presence of water using acetic acid (5%) as catalyst. The films were deposited onto glass substrates using the dip-coating method with a pulling speed of 10 cm/min. These films were annealed at 500 °C for about 1 h for oxide formation.

C. Electrode modification and immobilization of Urease-GLDH

Ten microliters (μL) of 1:1 molar mixture of urease and GLDH (1.0 mg/mL, in PB, 50 mM, pH 7.0) was immobilized onto a sol-gel TiO_2–CeO_2 nanocomposite electrode by the physisorption method.[25] The biochemical reaction using the mixed enzyme system is shown in Eq. (1). Prior to being used, the Urs-GLDH/TiO_2–CeO_2/ITO bioelectrode was allowed to dry overnight under desiccated conditions and then washed with phosphate buffer saline (PBS, 50 mM, pH 7.0, 0.9% NaCl) to remove any unabsorbed enzymes (Urs-GLDH) and stored in a desiccator at 25 °C when not in use.

$$\text{Urea urease} \rightarrow 2\,NH_4^+ + HCO_3^- \quad , \tag{1}$$

$$2\,NH_4^+ + \alpha\text{−ketoglutarate} + NADH \rightarrow \text{GLDH}\ 2- \text{Glutamate} + NAD^+ \quad , \tag{2}$$

$$NADH \rightarrow NAD^+ + 2e^- \quad . \tag{3}$$

D. Characterization of sol-gel-derived TiO_2–CeO_2/ITO electrode and Urs-GLDH/TiO_2–CeO_2/ITO bioelectrode

Phase identification of the fabricated sol-gel-derived TiO_2–CeO_2 nanocomposite film was accomplished by x-ray diffractometer using Cu K_α radiation (Rigaku, US) in the range 20°–70° (2θ scale). These sol-gel-derived TiO_2–CeO_2/ITO and Urs-GLDH/TiO_2–CeO_2/ITO bioelectrodes were further characterized by Fourier transform infrared (FTIR) spectrophotometer (Perkin-Elmer, model 2000, US) in the spectral range 400–4000 cm^{-1}. Atomic force microscopy (AFM) using a Veeco DICP2 instrument (US) was used to examine the surface morphology of TiO_2–CeO_2. Electrochemical data was obtained on an Autolab Potentiostat/Galvanostat (Eco Chemie, Utrecht, The Netherlands) using a three-electrodes cell containing Ag/AgCl as reference electrode, platinum (Pt) wire as auxiliary electrode, and ITO as a working electrode in PBS solution containing 5 mM $[Fe(CN)_6]^{3-/4-}$.

III. RESULTS AND DISCUSSION

A. X-ray diffraction analysis

Figure 1 shows the results of the x-ray diffraction (XRD) studies in 2θ range 20°–70° of the TiO_2–CeO_2 film deposited on glass substrate through the sol-gel chemical process calcined at 500 °C. It was found that a mixed phase of anatase, rutile, and brookite was present in this sample. It is known that phase transformation among brookite, anatase, and rutile occurs when titanium oxide is treated under high temperature. The diffraction peaks of the mixed phase of CeO_2-doped TiO_2 were marked as anatase (A), brookite (B), and rutile (R), respectively. The seven distinct diffraction peaks were observed at approximately 2θ = 22°, 31°, 36°, 38°, 46°,

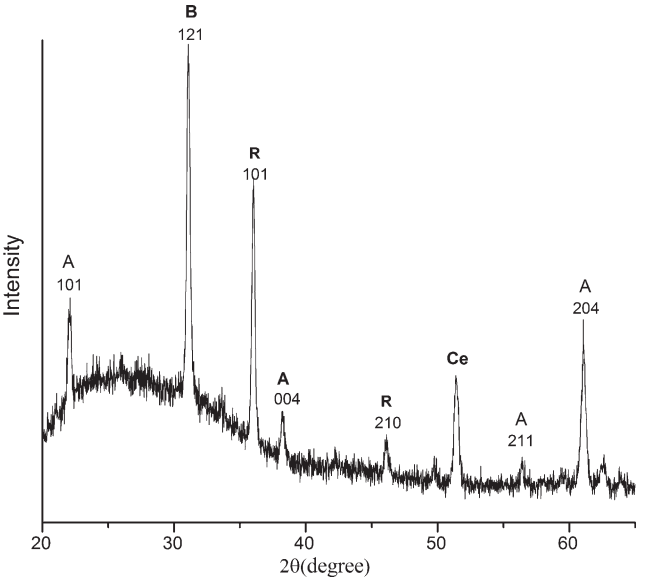

FIG. 1. XRD pattern of sol-gel-derived TiO_2–CeO_2 nanocomposite film.

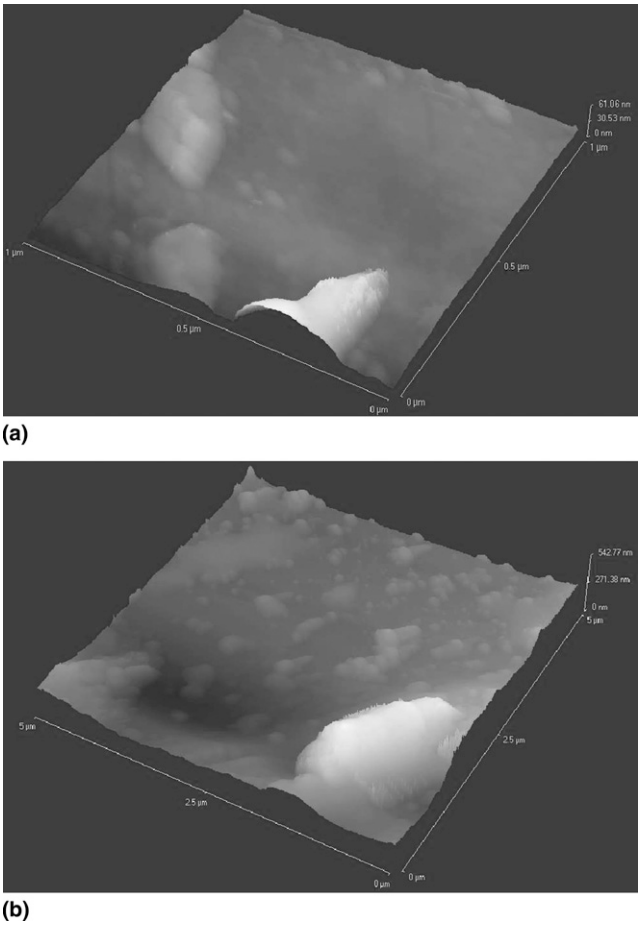

FIG. 2. AFM micrographs of (a) sol-gel-derived TiO_2–CeO_2/ITO nanocomposite electrode and (b) Urs-GLDH/TiO_2–CeO_2/ITO bioelectrode.

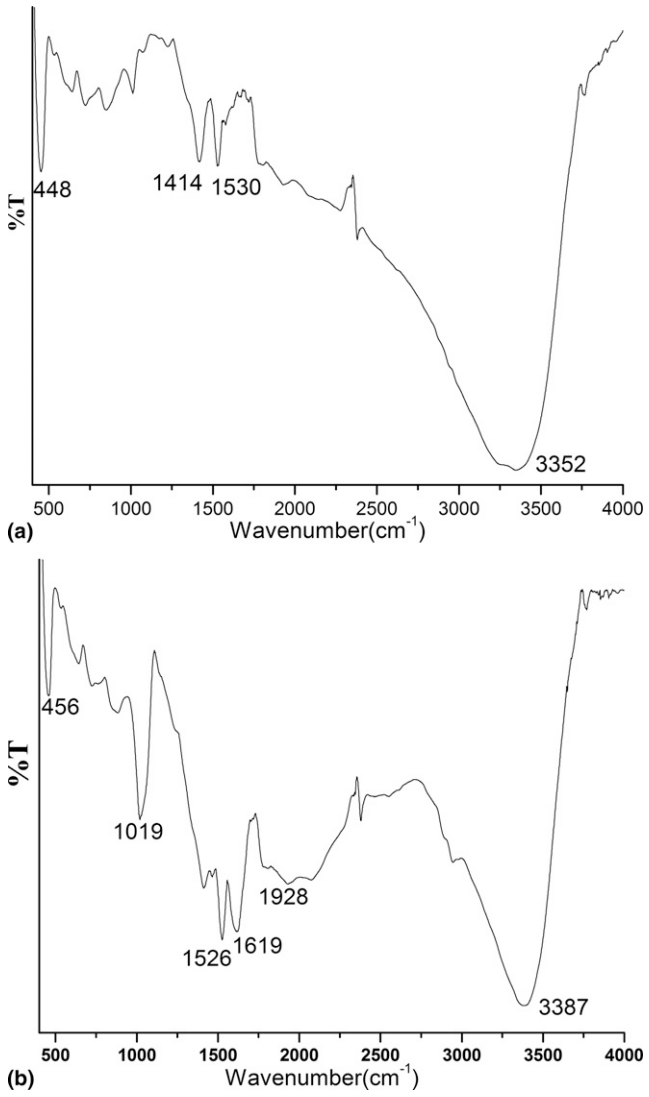

FIG. 3. FTIR spectra of (a) sol-gel-derived TiO_2-CeO_2/ITO nanocomposite electrode and (b) Urs-GLDH/TiO_2-CeO_2/ITO bioelectrode.

51.4°, and 61° and assigned to (101 for A), (121 for B), (101 for R), (004 for A), (210 for R), (101 for Ce), (211 for A), and (204 for A) reflections of mixed TiO_2–CeO_2 phase, respectively.[16,18–20,30] The average crystallite size was estimated by the analysis of the broadening of (121) and (101) reflections and was found to be 23 nm. The lattice constant (a) of the TiO_2 film calculated from the peak position found to be (a) = 0.460 Å, is slightly higher than that of bulk TiO_2 (0.455 Å) and is assigned to the distortion in the unit cell along the growth direction. In addition, an increase in the lattice constant reveals the lattice expansion effect resulting from the substitution of Ce^{4+} ions with decreasing particle size. The results imply that Ti atoms substitute Ce^{4+} ion in the TiO_2 lattice. Thus, the phase transformation of the resulting photocatalysts from anatase to rutile is exclusively induced by the thermal treatment rather than by the existence of cerium dopant in the TiO_2 lattice.

B. AFM

The AFM micrographs (Fig. 2) show surface topography of the prepared CeO_2 film revealing formation of the uniformly distributed spherical nanostructured thin film. The surface roughness of the TiO_2–CeO_2/ITO film determined as root mean square (rms) = 52 nm indicates high porosity and it decreases to 5 nm after enzyme (Urs-GLDH) immobilization. Globular structure is due to the presence of Urs-GLDH on the Urs-GLDH/TiO_2–CeO_2/ITO bioelectrode surface.

C. FTIR spectral studies

The TiO_2–CeO_2/ITO and Urs-GLDH/TiO_2–CeO_2/ITO bioelectrodes characterized by FTIR spectroscopy are shown in Fig. 3. A diffused band at 3352 cm^{-1} and two weak bands at 1414 and 1530 cm^{-1}, corresponding to the stretching and bending vibrations of the hydroxyl (O–H) group, respectively, are observed.[31,32] The appearance of these bands suggests the adsorption of moisture on the surface of nanostructured films. The FTIR

spectrum shows a sharp and intense band at around 448 cm^{-1} assigned to the Ti–O–Ce stretching band and indicates the deposition of TiO_2–CeO_2 film on the ITO surface.[31] Furthermore, the coadsorbed Urs-GLDH exhibits additional bands at 1928, 1616, 1525, and 1019 cm^{-1} corresponding to the stretching and bending vibrations of the amide, the functional groups indicating immobilization of Urs-GLDH on the nanocomposite matrix. FTIR results indicate Urs-GLDH binding with the nanocomposite via electrostatic interaction and hydrogen bond formation. The shift of the Ti–O–Ce stretching band toward a higher wave number (456 cm^{-1}) may be attributed to the electrostatic interaction and hydrogen bonding of the ceramic nanocomposite with the enzymes (Urs-GLDH).

D. Electrochemical impedance spectroscopy

Impedance spectroscopy is an effective means of probing the features of surface-modified electrodes. The complex impedance can be presented as the sum of the real, Z_{re}, and imaginary, Z_{im} components that originate mainly from the resistance and capacitance of the cell, respectively. The general electronic equivalent circuit (Randles and Ershler model), includes the ohmic resistance of the electrolyte solution, R_s, the Warburg impedance, D, resulting from the diffusion of ions from the bulk electrolyte to the electrode interface. The double-layer capacitance, C_{dl}, and charge-transfer resistance, R_{ct} exists, if a redox probe is present in the electrolyte solution, where R_s and D denote bulk properties of the electrolyte solution and diffusion features of the redox probe in solution, respectively. The other two components, C_{dl} and R_{ct}, depend on the dielectric and insulating features at the electrode/electrolyte interface. The double-layer capacitance consists of the constant capacitance of the unmodified electrode and a variable capacitance originating from an electrode surface modifier.[33] Table I gives the value of electrochemical impedance spectroscopy (EIS) parameters calculated from Fig. 4 based on an equivalent circuit.

In the Cole–Cole plot, the semicircle portion, observed at higher frequencies, corresponds to the electron-transfer-limited process, whereas the linear part is characteristic of the lower frequency range and represents the diffusion-limited electron-transfer process. As shown in Fig. 4, the semicircle diameter indicating the charge transfer resistance (R_{ct}) at the electrode interface of the bare ITO electrode is found to be 2.13 Ω. The increase of R_{ct} (8.11 Ω) value and the shift of semicircle to higher frequency after deposition of the TiO_2–CeO_2 layer on the ITO electrode is attributed to the low electrical conductivity of the TiO_2–CeO_2 nanobiocomposite material that provides slow electron transfer between enzyme and matrix. This result suggests that solution resistance (R_s) is slightly increased, but interfacial impedance (double-layer capacitance, C_{dl} and the charge transfer resistance, R_{ct}) is greatly increased after the deposition of TiO_2–CeO_2 film on the ITO electrode surface. The R_{ct} value decreases after enzymes (Urs and GLDH) are adsorbed onto the TiO_2–CeO_2/ITO electrode (R_{ct}, 4.25). Table I reveals that Warburg impedance (D), which represents the mass transfer, is enhanced after the immobilization of these enzymes (Urs-GLDH) on the TiO_2–CeO_2/ITO electrode surface, implying that enzyme molecules are indeed absorbed on TiO_2–CeO_2/ITO surfaces and induce impedance effects on the interface of the electrode surface. It is observed that the double-layer capacitance (C_{dl}) is decreased, indicating that a higher enzyme (Urs-GLDH) concentration enhances the adsorption of enzyme on the TiO_2–CeO_2/ITO modified electrode.

TABLE I. Electrochemical impedance characteristics of modified bioelectrodes.

Serial number	Electrodes	R_s (Ω)	R_{ct} (Ω)	D (Ω)	C_{dl} (nF)
1	Bare ITO	5.15	2.13	3.89	1.519
2	TiO_2–CeO_2/ITO	6.75	8.11	3.45	8.12
3	Urs-GLDH/TiO_2–CeO_2/ITO	6.83	4.25	4.46	1.34

E. Cyclic voltammetry studies

The changes of electrode behavior after surface modification with enzymes (Urs and GLDH) were studied by cyclic voltammetry (CV) in the presence of ferricyanide mediator. When the electrode surface is modified by the biocatalytic material, the change in the electron transfer kinetics of $[Fe(CN)_6]^{3-/4-}$ gives indication of the

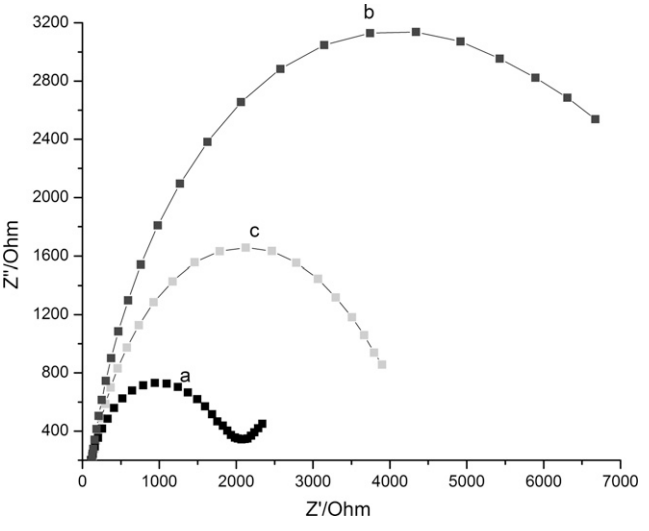

FIG. 4. Electrochemical impedance spectra of (a) bare ITO electrode, (b) sol-gel-derived TiO_2–CeO_2/ITO nanocomposite electrode, and (c) Urs-GLDH/TiO_2–CeO_2/ITO nanocomposite bioelectrode.

enzyme attachment. Figure 5 shows the cyclic voltammograms for Fig. 5(a) bare ITO electrode, Fig. 5(b) TiO_2-CeO_2/ITO electrode, and Fig. 5(c) Urs-GLDH/TiO_2-CeO_2/ITO bioelectrode in PBS (50mM, pH 7.0, 0.9% NaCl) containing 5 mM $[Fe(CN)_6]^{3-/4-}$ at a scan rate of 50 mVs^{-1}. As shown in Fig. 5, a well-defined redox couple of $[Fe(CN)_6]^{3-/4-}$ is observed on the bare ITO electrode (curve a). When the TiO_2–CeO_2/ITO nanocomposite layer is deposited on the ITO electrode, the peak current gradually decreases (curve b). The decrease in the peak potential after deposition of TiO_2–CeO_2 may be attributed to the hindrance of the electrons flow as a result of reduction in electrical conductivity of the nanostructured TiO_2–CeO_2/ITO electrode. In addition, the magnitude of the peak potential of the Urs-GLDH/TiO_2–CeO_2/ITO bioelectrode increases with peak-to-peak separation between the cathodic and anodic waves of the redox probe.

F. Response characteristics of biosensor

Figure 6 displays the response of the Urs-GLDH/TiO_2-CeO_2/ITO bioelectrode in PBS solution in the presence of NADH and α-KG and a successive addition of urea at an applied 50 mV/s scan rate. The peak current rises sharply with increased concentration of urea, with the maximum response approach at the concentration of 700 mg/dL after which it decreases. The sensor achieves 95% of the steady-state current in less than 5 s indicating fast electron exchange between the Urs-GLDH and TiO_2–CeO_2/ITO electrode. From the plot, two linear ranges are obtained for detection of urea (Fig. 6). The electrode is found to be linear in the range 10–100 mg/dL and 100–700 mg/dL with sensitivity of 0.078 μAcm^{-2} mM^{-1} and 0.901 $\mu Acm^{-2}mM^{-1}$ and correlation coefficients $R = 0.999$ and 0.994, respectively, and the detection limit of 0.166 μM with a relative standard deviation of 0.0022% using the Linweaver–Burke Eq. (1).[34]

$$I/I_{ss} = 1/I_{max} + K_m^{app}/I_{max}\,C \quad , \qquad (4)$$

where I_{ss} is the steady-state current after the addition of substrate, C is the bulk concentration of the substrate, and I_{max} is the maximum current measured under saturated substrate condition. The value of K_m, which is a reflection of enzymatic affinity, was found to be 4.8 mM. The lower K_m value with respect to glutaraldehyde-cross-linked urease-albumin gel (6.5 mM) and TMOS-based sol-gel (4.95 mM) indicates easier diffusion of substrate and product molecules into and out of

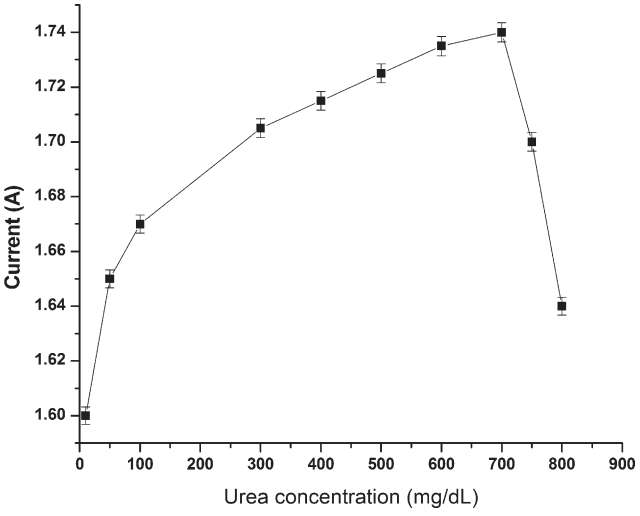

FIG. 6. Cyclic voltammetric characterization of Urs-GLDH/TiO_2–CeO_2/ITO nanocomposite bioelectrodes at various urea concentrations at 50 mV s^{-1} scan rate.

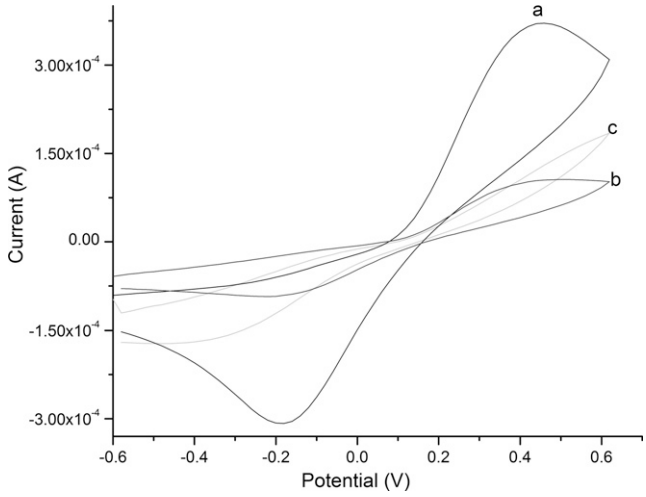

FIG. 5. Cyclic voltammograms of (a) bare ITO electrode, (b) sol-gel-derived TiO_2–CeO_2/ITO nanocomposite electrode, and (c) Urs-GLDH/TiO_2–CeO_2/ITO nanocomposite bioelectrode at 50 mV/s scan rate.

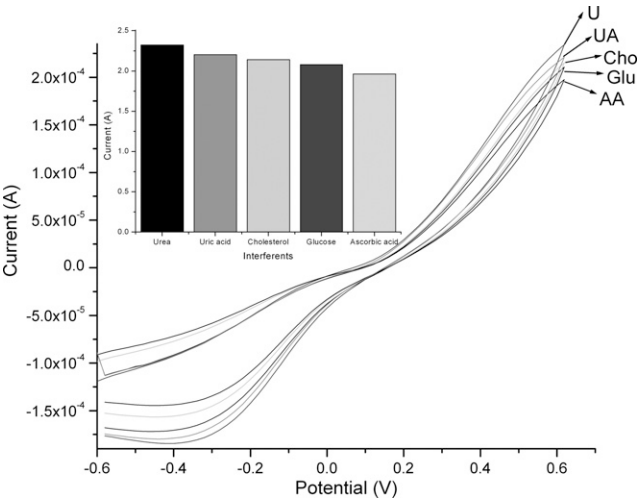

FIG. 7. Influence of interferents on the Urs-GLDH/TiO_2–CeO_2/ITO bioelectrode.

TABLE II. Characteristics of the sol-gel-derived TiO_2–CeO_2/ITO-based urea biosensor.

SN	Immobilization matrix	Method immobilization	Linearity (mM)	Detection limit (mM)	Shelf life	*K*m(mM)	Sensitivity	References
1	TMOS sol-gel	Physical entrapment	0.2–50 mM	0.2 mM	1 month	4.95	37.6 μS/mM	Lee et al.[36]
2	Silicate matrix by the sol-gel technique	Physical entrapment	0.03–30.0 mM	52 μg/mL	25 days	13.2	11.066 mV/M	Sahney et al.[37]
3	Sol-gel and screen-printed inter-digitated array	Physical entrapment	0.03–2.5	30 μM	< 25 days	Not reported	512 μS/mM	Lee et al.[38]
4	Sol-gel nile blue chromoionophore	Physical entrapment	20 mM	5.0–100 mM	100 days	Not reported	0.0060 Δ*A*/mM	Alqasaimeh et al.[39]
5	TiO_2–CeO_2/ITO	Physical entrapment	10–700 mg/dL	0.166 μM	2 month	4.8 mM	0.9165 $\mu Acm^{-2}mM^{-1}$	Present

the TiO_2–CeO_2 membrane and the feasible configuration of the enzyme in the nanocomposite matrix.[34]

The high affinity of Urs-GLDH to urea can be attributed to TiO_2–CeO_2 nanocomposite because of its biocompatibility, large surface area, and high electron communication capability. The value of ionization electron potential (IEP) of CeO_2 and urease are known to be 9.0 and 5.3, respectively.[35] Therefore, the TiO_2–CeO_2 matrix is positively charged in contrast to the enzymes that are negatively charged. Thus, immobilization of Urs-GLDH on the TiO_2–CeO_2 nanocomposite matrix is highly favored via electrostatic interaction.

The influence of pH of buffer on the response of the biosensor studied over the range 6.0–8.0 indicates that the current response increases with increase of pH of the substrate solution up to 7.0, after which it decreases. In view of the prime pH of the enzyme, the neutral pH was selected throughout this work (data not shown).

The influence of interferants was examined by mixing each of the interferants (ascorbic acid, uric acid, and cholesterol) with urea in equal concentration, and the results are depicted in Fig. 7. At 0.6V, it was observed that the response of the urea biosensor was not much affected due to the addition of ascorbic acid and negligible effect was observed by the addition of uric acid, cholesterol, and glucose, respectively. This TiO_2–CeO_2-based urea sensor exhibits sensitivity of 0.9165 $\mu Acm^{-2}mM^{-1}$ (Table II).

IV. CONCLUSIONS

The urea biosensor was fabricated by immobilizing Urs and GLDH onto the TiO_2–CeO_2 nanocomposite. This biosensor exhibits excellent performance characteristics, such as sensitivity (0.9165 $\mu Acm^{-2}mM^{-1}$) and reproducibility, wide linear range (10–700 mg/dL), low detection limit (0.166 μM), and long-term stability of about 2 months. The high sensitivity and specificity of the biosensor based on the TiO_2–CeO_2 nanocomposite toward urea make the interference of ascorbic acid, cholesterol, and glucose negligible. Efforts should be made to use this electrode for the detection of urea in blood serum.

ACKNOWLEDGMENTS

We thank Dr. Vikram Kumar, Director, National Physical Laboratory, New Delhi, India for the facilities. A.A. Ansari thanks Department of Biotechnology (DBT) for the award of the Research Associateship. We convey our special thanks to Mr. K.N. Sood for EDS characterization. We acknowledge Dr. P.R. Solanki for interesting discussions. The financial assistance received from various DST (GAP070932), DBT (GAP070832), and in-house Council of Scientific and Industrial Research (CSIR) projects are sincerely acknowledged.

REFERENCES

1. J. Wang: Electrochemical glucose biosensors. *Chem. Rev.* **108,** 814 (2007).
2. H. Lee, S.W. Yoon, E.J. Kim, and J. Park: In-situ growth of copper sulfide nanocrystals on multiwalled carbon nanotubes and their application as novel solar cell and amperometric glucose sensor materials. *Nano Lett.* **7,** 778 (2007).
3. S.P. Singh, S.K. Arya, P. Pandey, B.D. Malhotra, S. Saha, K. Sreenivas, and V. Gupta: Cholesterol biosensor based on rf sputtered zinc oxide nanoporous thin film. *Appl. Phys. Lett.* **91,** 063901 (2007).
4. R. Khan, A. Kaushik, P.R. Solanki, A.A. Ansari, M.K. Pandey, and B.D. Malhotra: Zinc oxide nanoparticles-chitosan composite film for cholesterol biosensor. *Anal. Chim. Acta* **616,** 207 (2008).
5. J.X. Wang, X.W. Sun, A. Wei, Y. Lei, X.P. Cai, C.M. Li, and Z.L. Dong: Zinc oxide nanocomb biosensor for glucose detection. *Appl. Phys. Lett.* **88,** 233106 (2006).
6. Y. Yang, H. Yang, M. Yang, Y. Liu, G. Shen, and R. Yu: Amperometric glucose biosensor based on a surface treated nanoporous ZrO_2/Chitosan composite film as immobilization matrix. *Anal. Chim. Acta* **525,** 213 (2004).
7. S. Zong, Y. Cao, Y. Zhou, and H. Ju: Zirconia nanoparticles enhanced grafted collagen tri-helix scaffold for unmediated biosensing of hydrogen peroxide. *Langmuir* **22,** 8915 (2006).
8. E. Topoglidis, Y. Astuti, F. Duriaux, M. Gratzel, and J.R. Durrant: Direct electrochemistry and nitric oxide interaction of heme

proteins adsorbed on nanocrystalline tin oxide electrodes. *Langmuir* **19,** 6894 (2003).
9. S. Liu and A. Chen: Coadsorption of horseradish peroxidase with thionine on TiO_2 nanotubes for biosensing. *Langmuir* **21,** 8409 (2005).
10. Y.T. Shi, R. Yuan, Y.Q. Chai, and X.L. He: Development of an amperometric immunosensor based on TiO_2 nanoparticles and gold nanoparticles. *Electrochim. Acta* **52,** 3518 (2007).
11. X. Xu, B. Tian, S. Zhang, J. Kong, D. Zhao, and B. Liu: Electrochemistry and biosensing reactivity of heme proteins adsorbed on the structure-tailored mesoporous Nb_2O_5 matrix. *Anal. Chim. Acta* **519,** 31 (2004).
12. K.J. Feng, Y.H. Yang, Z.J. Wang, J.H. Jiang, G.L. Shen, and R.Q. Yu: A nano-porous CeO_2/Chitosan composite film as the immobilization matrix for colorectal cancer DNA sequence-selective electrochemical biosensor. *Talanta* **70,** 561 (2006).
13. J. Yu and H. Ju: Preparation of porous titania sol-gel matrix for immobilization of horseradish peroxidase by a vapor deposition method. *Anal. Chem.* **74,** 3579 (2002).
14. T. Suzuki, I. Kosacki, and H.U. Anderson: Defect and mixed conductivity in nanocrystalline doped cerium oxide. *J. Am. Ceram. Soc.* **85,** 1492 (2002).
15. I. Kosacki, T. Suzuki, V. Petrovsky, and H.U. Anderson: Electrical conductivity of nanocrystalline ceria and zirconia thin films. *Solid State Ionics* **136–137,** 1225 (2000).
16. K. Nakagawa, Y. Murata, M. Kishida, M. Adachi, M. Hiro, and K. Susa: Formation and reaction activity of CeO_2 nanoparticles of cubic structure and various shaped CeO_2–TiO_2 composite nanostructures. *Mater. Chem. Phys.* **104,** 30 (2007).
17. T. Suzuki, I. Kosacki, and H.U. Anderson: Electrical conductivity and lattice defects in nanocrystalline cerium oxide thin films. *J. Am. Ceram. Soc.* **84,** 2007 (2001).
18. F.E. Ghodsi, F.Z. Tepehan, and G.G. Tepehan: Influence of pH on the optical and structural properties of spin coated CeO_2–TiO_2 thin films prepared by sol–gel process. *Surf. Sci.* **601,** 4497 (2007).
19. F.E. Ghodsi, F.Z. Tepehan, and G.G. Tepehan: Optical and electrochromic properties of sol-gel made CeO_2–TiO_2 thin films. *Electrochim. Acta* **44,** 3127 (1999).
20. C.O. Avellaneda and A. Pawlicka: Preparation of transparent CeO_2–TiO_2 coatings for electrochromic devices. *Thin Solid Films* **335,** 245 (1998).
21. Z. Hong, P. Zhang, A. Liu, L. Chen, X. Chen, and X. Jing: composites of poly(lactide-co-glycolide) and the surface modified carbonated hydroxyapatite nano-particles. *J. Biomed. Mater. Res. A* **81,** 515 (2007).
22. N.S. Hussain, M.A. Lopes, and J.D. Santos: A comparative study of CaO–P_2O_5–SiO_2 gels prepared by a sol-gel method. *Mater. Chem. Phys.* **88,** 5 (2004).
23. N.Q. Jia, Q. Zhou, L. Liu, M.M. Yan, and Z.Y. Jiang: Direct electrochemistry and electrocatalysis of horseradish peroxidase immobilized in sol–gel-derived tin oxide/gelatin composite films. *J. Electroanal. Chem.* **580,** 213 (2005).
24. S.Q. Liu, J.J. Xu, and H.Y. Chen: ZrO_2 gel-derived DNA-modified electrode and the effect of lanthanide on its electron transfer behavior. *Bioelectrochemistry* **57,** 149 (2002).
25. A. Gambhir, M. Gerard, A.K. Mulchandani, and B.D. Malhotra: Co-immobilization and characterization of urease and glutamate dehydrogenase in electro-chemically prepared polypyrrole-polyvinylsulphonate films. *Appl. Biochem. Biotechnol.* **96,** 249 (2001).
26. E. Topoglidis, A.E.G. Cass, G. Gilardi, S. Sadeghi, N. Beautmont, and J.R. Durrant: Protein adsorption on nanocrystalline TiO_2 films: An immobilization strategy for bioanalytical devices. *Anal. Chem.* **70,** 5111 (1998).
27. Y. Zhang, P. He, and N. Hu: Horseradish peroxidase immobilized in TiO_2 nanoparticle films on pyrolytic graphite electrodes: Direct electrochemistry and bioelectrocatalysis. *Electrochim. Acta* **49,** 1981 (2004).
28. H.J. Kim, S.H. Yoon, H.N. Choi, Y.K. Lyu, and W.Y. Lee: Amperomatric glucose biosensor based on sol-gel derived zirconia/nafion composite film as encapsulation matrix. *Bull. Korean Chem. Soc.* **27,** 65 (2006).
29. J.C. Chen, J.C. Chou, T.P. Sun, and S.K. Hsiung: Portable urea biosensor based on the extended-gate field effect transistor. *Sens. Actuators B* **91,** 180 (2003).
30. D. Reyes-Coronado, G. Rodriguez-Gattorno, M.E. Espinosa Pesqueira, C. Cab, R. de Coss, and G. Oskam: Phase-pure TiO_2 nanoparticles: Anatase, brookite and rutile. *Nanotechnology* **19,** 145605 (2008).
31. K. Nakamoto: *Infrared and Raman Spectra of Inorganic and Coordination Compounds*, 3rd ed. (John Wiley Interscience, New York, 1978).
32. Z.H. Cheng, A. Yasukawa, K. Kandori, and T. Ishikawa: FTIR study of adsorption of CO_2 on nonstoichiometric calcium hydroxyapatite. *Langmuir* **14,** 6681 (1998).
33. X. Chen, Y. Wang, J. Zhou, W. Yan, X. Li, and J.J. Hu: Electrochemical impedance immunosensor based on three-dimensionally ordered macroporous gold film. *Anal. Chem.* **80,** 2133 (2008).
34. R.A. Kamin and G.S. Wilson: Rotating ring-disk enzyme electrode for biocatalysis kinetic studies and characterization of the immobilized enzyme layer. *Anal. Chem.* **52,** 1198 (1980).
35. A.A. Ansari, P.R. Solanki, and B.D. Malhotra: Sol-gel derived nanostructured cerium oxide film for glucose sensor. *Appl. Phys. Lett.* **93,** 263901 (2008).
36. W.Y. Lee, K.S. Lee, T.H. Kim, M.C. Shin, and J.K. Park: Microfabricated conductometric urea biosensor based on sol-gel immobilized urease. *Electroanalysis* **12,** 78 (2000).
37. R. Sahney, B.K. Puri, and S. Anand: Enzyme coated glass pH-electrode: Its fabrication and applications in the determination of urea in blood samples. *Anal. Chim. Acta* **542,** 157 (2005).
38. W.Y. Lee, S.R. Kim, T.H. Kim, K.S. Lee, M.C. Shin, and J.K. Park:twb Sol-gel-derived thick-film conductometric biosensor for urea determination in serum. *Anal. Chim. Acta* **404,** 195 (2000).
39. M.S. Alqasaimeh, L.Y. Heng, and M. Ahmad: A urea biosensor from stacked sol-gel films with immobilized nile blue chromoionophore and urease enzyme. *Sensors* **7,** 2251 (2007).